Author(s): Vasala, Sami & Saadaoui, Hassan & Morenzoni, Elvezio & Chmaissem, Omar & Chan, Ting-Shan & Chen, Jin-Ming & Hsu, Ying-Ya & Yamauchi, Hisao & Karppinen, Maarit

Title: Characterization of magnetic properties of Sr2CuWO6 and Sr2CuMoO6

Year: 2014

Version: Final published version

Please cite the original version:

Vasala, Sami & Saadaoui, Hassan & Morenzoni, Elvezio & Chmaissem, Omar & Chan, Ting-Shan & Chen, Jin-Ming & Hsu, Ying-Ya & Yamauchi, Hisao & Karppinen, Maarit. 2014. Characterization of magnetic properties of Sr2CuWO6 and Sr2CuMoO6. Physical Review B. Volume 89, Issue 13. 134419/1-9. ISSN 1550-235X (electronic). DOI: 10.1103/physrevb.89.134419.

Characterization of magnetic properties of Sr_2CuWO_6 and Sr_2CuMoO_6

Sami Vasala,[1] Hassan Saadaoui,[2] Elvezio Morenzoni,[2] Omar Chmaissem,[3,4] Ting-Shan Chan,[5] Jin-Ming Chen,[5] Ying-Ya Hsu,[6] Hisao Yamauchi,[1] and Maarit Karppinen[1,*]

[1]*Department of Chemistry, Aalto University, FI-00076 AALTO, Finland*
[2]*Laboratory for Muon Spin Spectroscopy, Paul Scherrer Institute, CH-5232 Villigen PSI, Switzerland*
[3]*Department of Physics, Northern Illinois University, DeKalb, Illinois 60115, USA*
[4]*Materials Science Division, Argonne National Laboratory, Argonne, Illinois 60439, USA*
[5]*National Synchrotron Radiation Research Center, Hsinchu 30076, Taiwan*
[6]*Program for Science and Technology of Accelerator Light Source, National Chiao Tung University, Hsinchu 30076, Taiwan*

(Received 9 February 2014; revised manuscript received 4 April 2014; published 21 April 2014)

In this work we examine the low-temperature magnetic properties of the two double-perovskite compounds Sr_2CuWO_6 and Sr_2CuMoO_6 using magnetic susceptibility, muon spin rotation and relaxation, and neutron powder diffraction measurements. Additionally, the most relevant spin exchange interaction constants are derived from *ab initio* electronic structure calculations, aided by x-ray absorption spectroscopy. The compounds exhibit quasi-two-dimensional magnetic properties, with broad maxima at $T_{max} = 83$ and 95 K for Sr_2CuWO_6 and Sr_2CuMoO_6, respectively. However, three-dimensional long-range order takes place below $T_N = 24(1)$ and 28(2) K for Sr_2CuWO_6 and Sr_2CuMoO_6, respectively. Our results show that the low-dimensional magnetic correlations are mainly due to the significant next-nearest-neighbor interactions in the *ab* plane of the double-perovskite structure, whereas three-dimensional long-range magnetic order is caused by weaker next-nearest-neighbor interactions along the *c* axis. Next-nearest-neighbor interactions are also slightly frustrated by weaker nearest-neighbor interactions within the *ab* plane. Based on these results we predict the low-temperature magnetic structure in these compounds to be type-II antiferromagnetic order of the double-perovskite lattice.

DOI: 10.1103/PhysRevB.89.134419 PACS number(s): 61.05.fm, 71.20.Ps, 75.50.Ee, 76.75.+i

I. INTRODUCTION

Low-dimensional magnetism has been at the center of solid-state physics for several decades. Interest in this phenomenon stems partly from the fact that the parent phases of high-T_c copper-oxide superconductors are two-dimensional antiferromagnets (AFMs). Moreover, superconductivity is believed to be connected to short-range magnetic fluctuations that exist just before the materials become superconducting [1–3]. The AFM copper oxides have a square lattice of $S = \frac{1}{2}$ Cu^{II} ions separated by oxide ions, and possess strong in-plane superexchange interactions with $J \approx 130$ meV ($\sim$1500 K) [4,5]. Such strong interactions prevent the studies of some properties, such as magnetic specific heat, at temperatures of the order of J [5]. Therefore, finding examples of similar square lattice compounds with weaker interactions is of current interest for basic research.

The B-site ordered double-perovskite oxides $A_2CuB''O_6$, where A = Sr or Ba and B'' is a diamagnetic hexavalent ion such as Mo, Te, W, or U, crystallize in a tetragonal structure with short Cu-O bonds in the *ab* plane and long Cu-O bonds along the *c* axis, due to the cooperative Jahn-Teller (JT) effect of the octahedrally coordinated d^9 Cu^{II} ion (see, e.g., Ref. [6] and the references therein). While structurally three-dimensional, many of these compounds show low-dimensional magnetic properties: in an ideally ordered $A_2CuB''O_6$ compound, the *ab* planes have a square-centered array of Cu^{II}, with the half-filled Cu $3d_{x^2-y^2}$ orbitals ordered into the *ab* planes by the JT distortion. This creates magnetic interactions between the neighboring Cu ions within the *ab* planes. As the d_{z^2}, d_{yz}, and d_{zx} orbitals of Cu^{II} are all filled, the magnetic interactions along the *c* axis are expected to be weak, which renders the magnetic interactions quasi-two-dimensional [6].

What makes these $A_2CuB''O_6$ compounds of particular interest is that the magnetic interactions, in double perovskites where the magnetic ions are separated by an array of diamagnetic O-B''-O ions, are generally an order of magnitude weaker than in compounds where the magnetic ions are only separated by oxygen. This is due to the intervening diamagnetic B'' ion and the long distances between the magnetic ions [7,8]. Thus, it becomes possible to study the low-temperature low-dimensional magnetic properties in this class of compounds. Additionally, the diamagnetic B'' ion adds an extra degree of freedom for creative chemical substitutions, which can be used to modify and tune the magnetic properties of these materials.

In a previous study, we reported the synthesis of a series of $Sr_2Cu(W_{1-x}Mo_x)O_6$ compounds [6]. These materials all exhibit a broad maximum in their magnetic susceptibility, indicative of low-dimensional antiferromagnetic behavior. We determined the susceptibility maxima T_{max} at 83 and 95 K and the Curie-Weiss temperatures θ of -116 and ~ -300 K for Sr_2CuWO_6 and Sr_2CuMoO_6, respectively. Moreover, susceptibility measurements showed no clear indication of long-range magnetic order at temperatures down to 5 K. However, another similar quasi-two-dimensional magnetic compound, Ba_2CuWO_6, has been found by muon spin rotation and relaxation (μSR) and neutron powder diffraction (NPD) measurements to exhibit three-dimensional long-range AFM order below $T_N = 28$ K [9]. This temperature is significantly different than the susceptibility maximum ($T_{max} \approx 100$ K [8,10]) or the Weiss temperature ($\theta = -249$ K [8] or $\theta = -178$ K [10]), suggesting that the interactions along the

*Corresponding author: maarit.karppinen@aalto.fi

c axis, responsible for the long-range order, are relatively weak but not negligible.

In this work we report low-temperature three-dimensional magnetic ordering for the two quasi-two-dimensional end members Sr_2CuWO_6 and Sr_2CuMoO_6 of the $Sr_2Cu(W_{1-x}Mo_x)O_6$ phase diagram. As with Ba_2CuWO_6, the ordering temperature is relatively low compared to the overall energy scale of the magnetic interactions. We use magnetic susceptibility measurements, μSR, and NPD to study the details of these compounds at low temperatures. In addition, we calculate the most relevant spin exchange interaction constants for $Sr_2Cu(W,Mo)O_6$ from first principles using density-functional theory (DFT) electronic-structure calculations. The on-site Coulomb correlation of the localized Cu $3d$ electrons is taken into account using the DFT + U method, and in this work we use x-ray absorption spectroscopy (XAS) data as an experimental reference in order to estimate the required value of U. Based on these computational results we explain the magnetic properties of the two compounds.

II. EXPERIMENTAL DETAILS

The Sr_2CuWO_6 sample was synthesized by solid-state reaction of a stoichiometric mixture of $SrCO_3$, CuO, and WO_3 powders. The mixture was thoroughly ground in an agate mortar together with ethanol and then calcined for 12 hours in air at 900 °C. The sample was then reground, pressed into pellets, and sintered twice in air at 1000 °C for 24 hours. The Sr_2CuMoO_6 sample was synthesized under high pressure (HP). A stoichiometric mixture of $SrCO_3$, CuO, and MoO_3 powders was ground and calcined at 900 °C for 12 h in air. The calcined powder was sealed in a gold capsule and treated in a cubic-anvil HP apparatus (Riken-Seiki) at about 4 GPa and 900 °C for 60 minutes. Additionally, a series of $Sr_2Cu(W_{1-x}Mo_x)O_6$ samples with $x = 0$, 0.1, 0.2, 0.3, 0.4, 0.5, 0.8, and 1 were synthesized for the XAS measurements, as described elsewhere in more detail [6].

DC magnetic susceptibility was measured between 5 and 300 K using a superconducting quantum interference device (SQUID, Quantum Design: MPMS-XL5) under a magnetic field of 10 kOe in both field-cooled (FC) and zero-field-cooled (ZFC) measurement modes.

Muon spin rotation and relaxation (μSR) experiments were performed at the General Purpose Spectrometer (GPS) instrument located at the πM3 beamline of the Paul Scherrer Institute, Switzerland. Zero-field (ZF) measurements of Sr_2CuWO_6 and Sr_2CuMoO_6 at various temperatures between 4 and 35 K allowed us to investigate the local magnetic properties and the appearance of long-range order. The data were analyzed using the program MUSRFIT [11]. The spectra for both compounds were fitted in the time range of $t = 0.01$–1 μs with the function

$$A(t) = A_{\text{sample}} G_{\text{KT}}[f_L e^{-\lambda_L t} + f_F e^{-\lambda_F t} + (1 - f_L - f_F) \times \cos(\gamma_\mu B t) e^{-\lambda_T t}] + A_{\text{bkg}}, \quad (1)$$

where A_i, f_i, and λ_i are the initial asymmetries, fractions, and relaxation rates of different components, respectively. $\gamma_\mu = 85.16 \times 10^3$ rad s^{-1} G^{-1} is the muon gyromagnetic ratio and B is the local magnetic field felt by the muon. The total initial asymmetry was determined as $A_{\text{total}} = 0.22$ and the initial sample asymmetry was $A_{\text{sample}} = 0.95 A_{\text{total}}$. $A_{\text{bkg}} = 0.05 A_{\text{total}}$ takes into account a small nonrelaxing background. The sample signal had a contribution from nuclear moments, taken into account by the Kubo-Toyabe function [12] G_{KT} of $\sigma = 0.05$ μs^{-1}.

Time-of-flight (TOF) neutron powder diffraction (NPD) data were collected for Sr_2CuWO_6 at the BL-11A POWGEN beamline, Spallation Neutron Source (SNS), Oak Ridge National Laboratory. Two frames were collected with the center wavelength of 1.066 Å for full structural refinements, and 2.665 Å for the detection of possible magnetic reflections at higher d-spacing values. A sample of ~5 g was packed into a vanadium sample holder filled with helium gas. Measurements were performed at temperatures of 10, 100, and 300 K. Rietveld refinements were performed with FULLPROF [13] using a d-spacing range from 0.53 to 4.60 Å. The magnetic reflections of these compounds are expected to be quite weak, similarly to Ba_2CuWO_6 [9]. Therefore, no NPD measurements were performed for the high-pressure synthesized Sr_2CuMoO_6 sample as not much material was available for adequate data collection and detection of possible magnetic reflections.

Oxygen K-edge x-ray absorption spectroscopy (XAS) measurements were performed for $Sr_2Cu(W_{1-x}Mo_x)O_6$ samples with $x = 0$, 0.1, 0.2, 0.3, 0.4, 0.5, 0.8, and 1 at the BL-20A high-energy spherical grating monochromator (HSGM) beamline at the National Synchrotron Radiation Research Center (NSRRC), Hsinchu, Taiwan. The spectra were recorded in total-electron-yield (TEY) mode and normalized for comparison.

III. COMPUTATIONAL DETAILS

The spin exchange interactions of a magnetic solid can be modeled with exchange constants J_{ij} between spins S_i and S_j at sites i and j by the spin Hamiltonian

$$\hat{H} = -\sum_{i<j} J_{ij} \hat{S}_i \cdot \hat{S}_j. \quad (2)$$

In the $Sr_2Cu(W,Mo)O_6$ compounds W and Mo are hexavalent and diamagnetic. Therefore, only interactions between the Cu^{II} ions need to be considered. We calculate the four most relevant exchange constants for both Sr_2CuWO_6 and Sr_2CuMoO_6, as presented in Fig. 1: J_1 and J_2 are the nearest-neighbor (NN) and next-nearest-neighbor (NNN) exchange constants in the ab plane, respectively. J_3 and J_4 are the NN and NNN interplanar exchange constants along the c axis, respectively.

In order to calculate the magnetic exchange constants J_1-J_4, we use the so-called "mapping method" [14–17]. We construct five different magnetic ordering models: one ferromagnetic (FM), and four different antiferromagnetic (AFM) configurations, as presented schematically in Fig. 2. Assuming that the total energy of the system can be divided into a nonmagnetic part with energy E_0 and a magnetic part whose energy is determined by the Hamiltonian in Eq. (2), the total energies per two formula units for the five ordered states

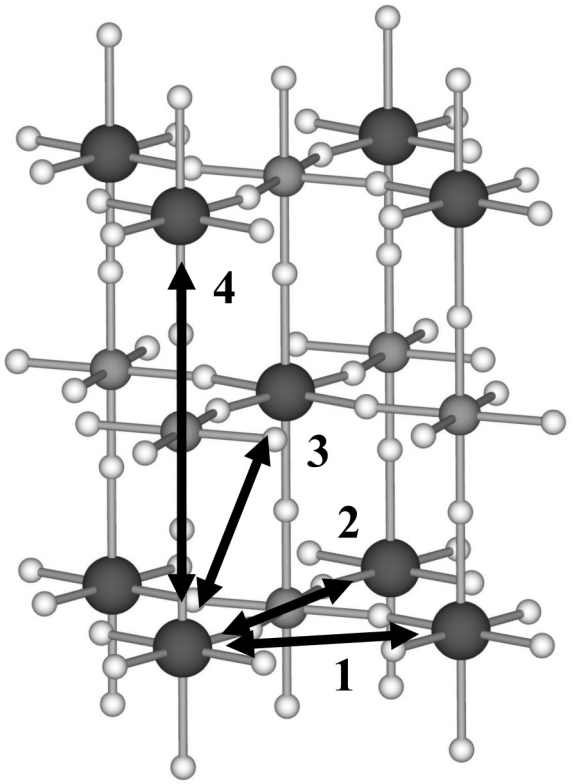

FIG. 1. Schematic of the exchange constants J_1-J_4 between Cu ions in the $Sr_2Cu(W,Mo)O_6$ double perovskites. Large dark-gray spheres are Cu, smaller light-gray spheres are W/Mo, and small white spheres are O. Sr is omitted from view for clarity.

can be written as

$$E_{\mathrm{FM}} = E_0 + (-4J_1 - 4J_2 - 8J_3 - 2J_4)S^2, \quad (3)$$

$$E_{\mathrm{AFM1}} = E_0 + (-4J_1 - 4J_2 + 8J_3 - 2J_4)S^2, \quad (4)$$

$$E_{\mathrm{AFM2}} = E_0 + (4J_1 - 4J_2 - 2J_4)S^2, \quad (5)$$

$$E_{\mathrm{AFM3}} = E_0 + (4J_2 - 2J_4)S^2, \quad (6)$$

$$E_{\mathrm{AFM4}} = E_0 + (-4J_1 - 4J_2 + 2J_4)S^2, \quad (7)$$

where $S = \frac{1}{2}$ is the spin moment of the Cu^{II} ion. The total energies can be determined from *ab initio* electronic band-structure calculations. From the calculated total energies the exchange constants can be solved as

$$J_3 = (E_{\mathrm{AFM1}} - E_{\mathrm{FM}})/16S^2, \quad (8)$$

$$J_1 = (E_{\mathrm{AFM2}} - E_{\mathrm{FM}} - 8J_3S^2)/8S^2, \quad (9)$$

$$J_2 = (E_{\mathrm{AFM3}} - E_{\mathrm{FM}} - 4J_1S^2 - 8J_3S^2)/8S^2, \quad (10)$$

$$J_4 = (E_{\mathrm{AFM4}} - E_{\mathrm{FM}} - 8J_3S^2)/4S^2. \quad (11)$$

Additionally, in order to compare the overall magnitude of the calculated J_{ij} with the experimental results, the Weiss constant θ can be calculated from the exchange constants using the mean-field approximation:

$$\theta = \frac{S(S+1)}{3k_B} \sum_i z_i J_i, \quad (12)$$

where k_B is the Boltzmann constant and z_i is the number of interactions J_i.

In order to determine the total energies of the different magnetic orderings, density-functional theory (DFT) calculations for Sr_2CuWO_6 and Sr_2CuMoO_6 were performed with the full-potential linearized augmented plane wave (FP-LAPW) code ELK [18] using the generalized gradient approximation (GGA) and the Perdew-Burke-Ernzerhof (PBE) functional. A plane wave cutoff of $|\boldsymbol{G} + \boldsymbol{k}|_{\max} = 6.0/R_{\min}$ a.u.$^{-1}$ was used, where $R_{\min}$ is the smallest muffin-tin radius in the unit cell, and the total energy was converged within 10^{-6} Ha. For the density of states (DOS) calculations, a tetragonal single unit cell was used, with an $8 \times 8 \times 6$ Monkhorst-Pack k-point grid. In order to calculate the total energies of the different magnetic orderings, larger $2 \times 2 \times 1$ or $1 \times 1 \times 2$ supercells were used, with either $4 \times 4 \times 6$ or $8 \times 8 \times 3$ Monkhorst-Pack k-point grids, respectively.

In previous work we showed that the empty Cu $3d$–O $2p$ band of these compounds is pushed up in energy, above the W $5d$–O $2p$ or Mo $4d$–O $2p$ conduction band edge, by strong on-site Coulomb correlation of the localized Cu $3d$ electrons [6]. This correlation was taken into account by DFT + U calculations with the U-I formalism, using the "around mean field" correction for double counting. The value of U was estimated from comparison with XAS data, as discussed later. The value of the Stoner intra-atomic exchange parameter I is not expected to be greatly affected by the crystal structure, and was thus chosen as 0.90 eV, a typical

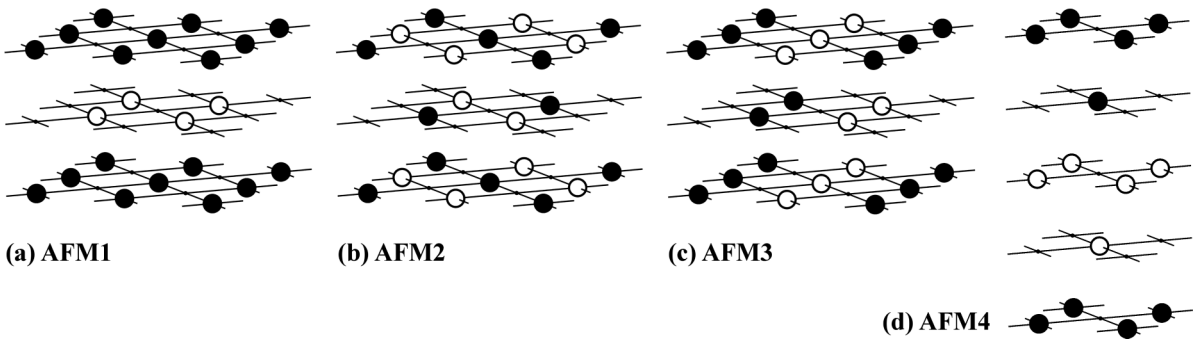

FIG. 2. Schematic of the four AFM orderings used in calculating the magnetic exchange constants of $Sr_2Cu(W,Mo)O_6$. Black spheres correspond to Cu ions with spin up, and white spheres to Cu ions with spin down. Other ions and the long bonds along c axis are omitted from view for clarity.

value for 3*d* transition metals [19,20]. No U term was used for W or Mo, as the ions are hexavalent, and the *d* electrons are all delocalized due to hybridization with the O 2*p* states [16].

The XAS spectrum for Sr_2CuWO_6 was simulated with CASTEP [21], a pseudopotential–plane wave DFT code, using GGA-PBE and CASTEP's "on-the-fly" generated pseudopotentials. A plane wave cutoff of 610 eV was used. A reduced primitive unit cell was used, with a $5 \times 5 \times 7$ Monkhorst-Pack k-point grid. The structural parameters from Rietveld refinement were used for all the calculations without further geometry optimization.

IV. RESULTS

The magnetic susceptibilities of Sr_2CuWO_6 and Sr_2CuMoO_6 as a function of temperature are shown in Fig. 3. As we have reported before, the curves show broad maxima around $T_{max} = 83$ and 95 K for Sr_2CuWO_6 and Sr_2CuMoO_6, respectively, with no clear indication of a transition to a long-range-ordered magnetic state [6]. However, the susceptibility curve of Sr_2CuMoO_6 shows a tiny kink at around 30 K, and the second derivative of it (shown in the inset of Fig. 3) reveals kinks at around 20–30 K for both Sr_2CuWO_6 and Sr_2CuMoO_6. Similar kinks could be seen for all the samples in the $Sr_2Cu(W_{1-x}Mo_x)O_6$ series. These features may indicate a transition to a long-range-ordered state, but the susceptibility data are not conclusive enough to confirm such transitions.

To unambiguously establish the presence of a transition to a long-range-ordered state we performed μSR experiments for Sr_2CuWO_6 and Sr_2CuMoO_6. In μSR, the time evolution of the polarization of a muon ensemble stopped in the sample is measured. Figure 4 shows the ZF μSR spectra measured for Sr_2CuWO_6 at three different temperatures as an example. In the case of a magnetically ordered state, the spins of the initially 100% polarized muons will precess in the local field. The time evolution of their polarization then shows an oscillating component with a frequency proportional to the local field at the stopping site, described by the

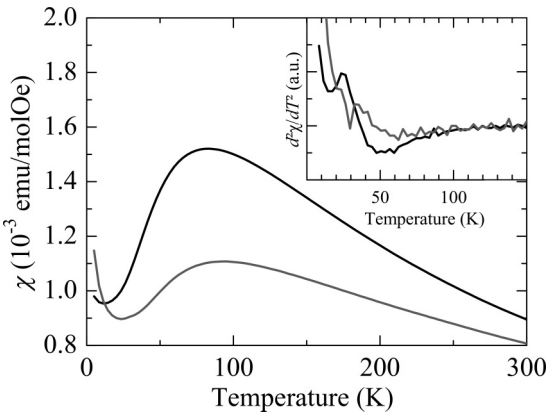

FIG. 3. Magnetic susceptibility as a function of temperature for Sr_2CuWO_6 (black) and Sr_2CuMoO_6 (gray). As the ZFC and FC curves overlap completely, only ZFC curve is shown. Inset: Second derivative of the magnetic susceptibility.

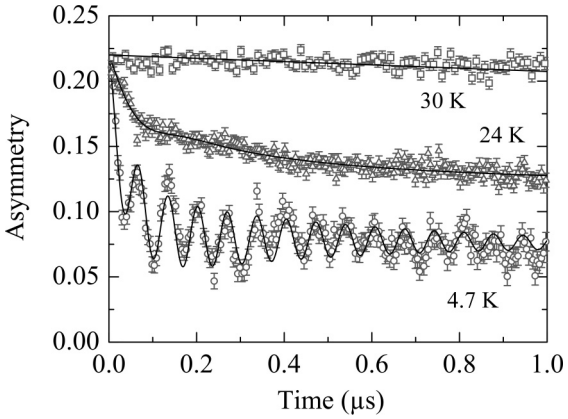

FIG. 4. ZF μSR spectra measured for Sr_2CuWO_6 at different temperatures. The solid black curves are the results from fitting with Eq. (1).

$\cos(\gamma_\mu Bt)e^{-\lambda_T t}$ component in Eq. (1). A clear spontaneous oscillation appearing below 24(1) and 28(2) K for Sr_2CuWO_6 and Sr_2CuMoO_6, respectively, was observed in the μSR spectra. These temperatures can be assigned as the Néel temperatures T_N where long-range magnetic order takes place. Additionally, at the same temperature the onset of a fast initial depolarization (the $e^{-\lambda_F t}$ component) of the signal was observed. This reflects a fraction of muons (about 15%) probing a broad distribution of strong magnetic fields, probably due to a distribution of muon sites or to muons stopping in intergrain regions. The decay of the spectra at late times to a "tail" with an amplitude of 1/3 of the initial amplitude clearly shows that the samples are fully magnetically ordered at low temperatures. Above T_N the only contribution to the signal was from the slowly decaying $e^{-\lambda_L t}$ component, with $\lambda_L = 0.06\ \mu s^{-1}$ at all temperatures, and the samples appeared paramagnetic, with no sign of quasistatic short-range order.

Figure 5 displays the temperature dependence of the local magnetic field as determined from fittings of the μSR spectra for Sr_2CuWO_6 and Sr_2CuMoO_6. This quantity is proportional to the size of the spontaneously ordered moment and can be taken as a measure of the magnetic order

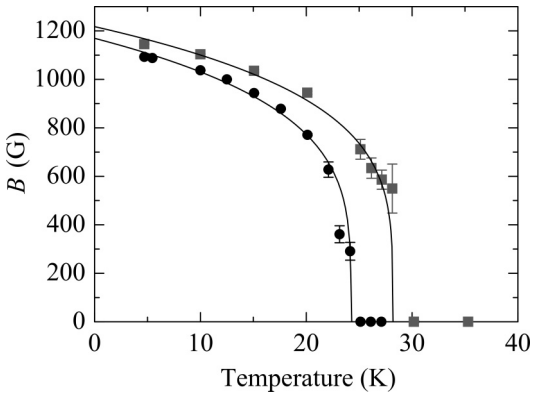

FIG. 5. Temperature dependence of the local field in Sr_2CuWO_6 (black circles) and Sr_2CuMoO_6 (gray squares). The solid black lines are the results from fitting with the critical exponent function, Eq. (13).

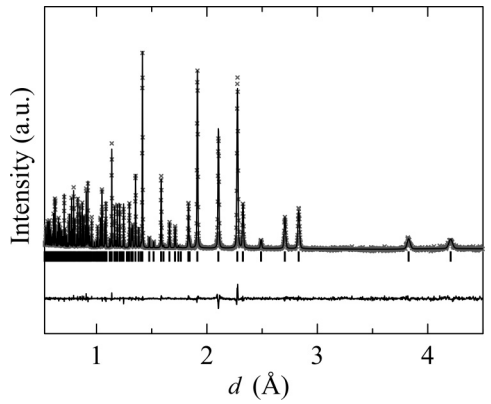

FIG. 6. Rietveld refinement results for NPD measurements of Sr_2CuWO_6 at 10 K with neutron wavelength of 1.066 Å.

parameter. The data were fitted with the critical exponent function

$$B = B_0\left(1 - \frac{T}{T_N}\right)^{\beta}, \tag{13}$$

where B_0 is the field at $T = 0$ K and β is the critical exponent. The data could be fitted well in the whole temperature range below T_N, as shown in Fig. 5, resulting in critical exponents of $\beta = 0.23(1)$ for both of the compounds. Such low values of the exponent would suggest a development of low-dimensional magnetic order [22]. However, restricting the fitting to a more limited temperature range near T_N, where Eq. (13) is more applicable, gave critical exponents in the range $\beta = 0.3$–0.4. The number of data points near T_N was not high enough for a more detailed analysis, but these values of β are consistent with values found for 3D Heisenberg antiferromagnets [23].

The NPD patterns of Sr_2CuWO_6 were analyzed by Rietveld refinement in order to determine the crystal structure at various temperatures. Figure 6 shows the 10 K case as an example and the refinement results of the 10, 100, and 300 K data are collected in Table I. The 300 K results are essentially identical to our previous results using laboratory x-ray diffraction [6]. The refinement results showed no sign of structural transitions with decreasing temperature, and the crystal structure of Sr_2CuWO_6 remains tetragonal $I4/m$ down to 10 K. The response of the crystal structure to the decreasing temperature is very subtle: the unit cell parameter a decreases slightly, whereas the parameter c remains practically constant. In addition, the Cu-O and W-O bond lengths remain almost constant, and the main change in the structure with decreasing temperature is the decrease in the Cu-O1-W bond angle within the ab plane, due to rotation of the CuO_6 octahedra along the c axis. NPD measurements were also done with the neutron center wavelength frame of 2.665 Å in order to better resolve any possible magnetic reflections related to the long-range order detected by μSR. However, comparing the pattern measured at 10 K, below T_N, to the one measured at 100 K did not show any clear new reflections or changes in peak intensities that could be assigned to magnetic order.

TABLE I. Rietveld refinement results for Sr_2CuWO_6 NPD data with space group $I4/m$.

T (K)	10	100	300
a (Å)	5.41254(4)	5.41459(5)	5.42911(6)
c (Å)	8.41577(8)	8.41552(8)	8.4159(1)
V (Å^3)	246.545(4)	246.724(4)	248.059(5)
Sr (0, 0.5, 0.25)			
B (Å^2)	0.20(1)	0.28(1)	0.68(1)
Cu (0, 0, 0.5)			
B (Å^2)	0.15(1)	0.18(1)	0.36(2)
W (0, 0, 0)			
B (Å^2)	0.14(2)	0.19(2)	0.38(3)
O1 (x, y, 0)			
x	0.2030(1)	0.2036(1)	0.2076(2)
y	0.2901(1)	0.2898(1)	0.2868(2)
B (Å^2)	0.37(1)	0.43(1)	0.75(2)
O2 (0, 0, z)			
z	0.22760(7)	0.22755(7)	0.2267(1)
B (Å^2)	0.38(2)	0.46(2)	0.87(3)
Cu-O1 (Å)	1.9684(7)	1.9675(8)	1.965(1)
Cu-O2 (Å)	2.2925(6)	2.2928(7)	2.300(1)
W-O1 (Å)	1.9164(7)	1.9177(8)	1.922(1)
W-O2 (Å)	1.9154(6)	1.9150(7)	1.908(1)
Cu-O1-W (°)	160.24(8)	160.43(8)	162.0(1)
R_p (%)	8.88	8.81	10.8
R_{wp} (%)	5.55	5.72	7.96
R_{Bragg} (%)	1.76	1.69	2.68
χ^2	5.47	5.47	7.49

In order to calculate the exchange interaction constants J_{ij} from first principles, as discussed in Sec. III, a value for the on-site Coulomb correlation energy U is required. Typically several different values of U are tested in order to divulge its effect on the exchange constants. Another possibility is to compare the calculations to experimental data, and choose a value of U that reproduces the measured properties. In this work we use XAS data as an experimental reference in order to estimate the value of U. XAS essentially probes the empty densities of states above the Fermi level by exciting an electron from a core level into an unoccupied state. Therefore comparing DOS calculated with different values of U to a measured XAS spectrum, we can estimate the required value of U. In the case of perovskite oxide materials, the O K-edge XAS is optimal for such comparison, as the O $2p$ orbitals are hybridized with all of the cations, and the spectrum therefore contains information about the empty states of all the ions.

Figure 7(a) shows the measured O K-edge XAS spectra for the $Sr_2Cu(W_{1-x}Mo_x)O_6$ samples with various Mo contents x from 0 to 1. The most relevant part of the spectra for our purposes is the multipeak-like absorption feature seen at 528–533 eV, which changes shape with increasing Mo content x. At the same time, the absorption edge moves to lower energies by about 0.8 eV when moving from Sr_2CuWO_6 to Sr_2CuMoO_6, comparable to the decrease in the direct-allowed optical band gap of 0.84 eV determined in our previous work [6]. For the samples with $x = 0.0$–0.5, the absorption

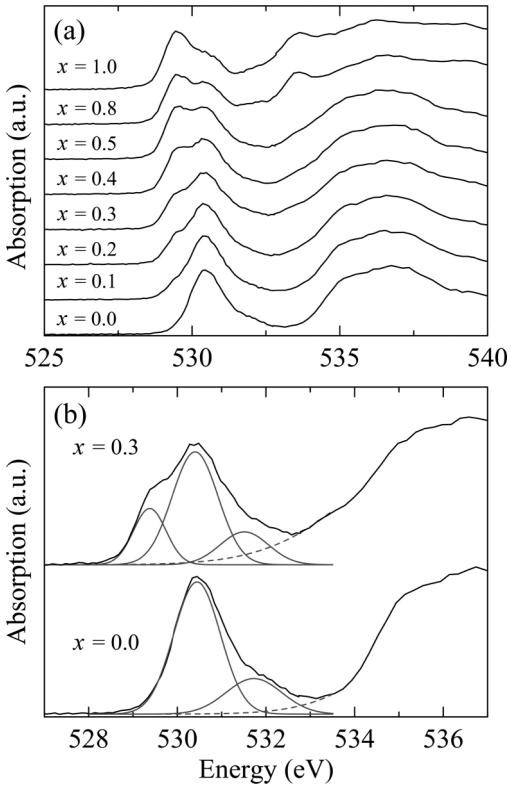

FIG. 7. (a) XAS spectra for $Sr_2Cu(W_{1-x}Mo_x)O_6$ samples with $x = 0.0$–0.5, 0.8, and 1.0. (b) Examples of Gaussian peak fittings to the XAS spectra of samples with $x = 0.0$ and 0.3.

feature at 528–533 eV could be fitted with Gaussian peaks, as shown as an example for samples $x = 0$ and 0.3 in Fig. 7(b). The high-pressure synthesized $x = 0.8$ and 1 (Sr_2CuMoO_6) samples contained impurity phases, most notably $SrMoO_4$ (∼5%), which caused additional features overlapping those of $Sr_2Cu(W,Mo)O_6$. Thus, these two samples could not be used for more detailed analysis.

For the $x = 0$ sample (Sr_2CuWO_6), two peaks were found: a large one with a center position at 530.4 eV and a smaller one at 531.2 eV, corresponding to a shoulder at the high-energy side of the larger peak. Figure 8 shows a comparison of the measured O K-edge XAS spectrum of Sr_2CuWO_6 with a simulated XAS spectrum and calculated DOS with $U = 0$ eV. Note that the calculated XAS spectrum and DOS in Fig. 8 are shifted in energy to match the measured spectrum, as the calculations yield the spectra relative to the Fermi level, instead of absolute absorption energy. We can see that most of the features of the calculated and measured spectra agree quite well, although the calculated results are slightly compressed in the energy scale compared to the experimental results. This is due to the well-known "scaling problem," caused by the inadequacy of ground-state calculations to describe the high-energy states [24]. The large absorption peak seen in the experimental XAS spectrum at 530.4 eV corresponds to the empty W 5d–O 2p band. The major difference in the calculated spectrum compared to the experimental one is the peak around 582 eV, which is not seen in the measured spectrum. The DOS shows that this peak originates from the empty Cu 3d–O 2p band. Moreover, the small shoulder seen at 531.2 eV in the

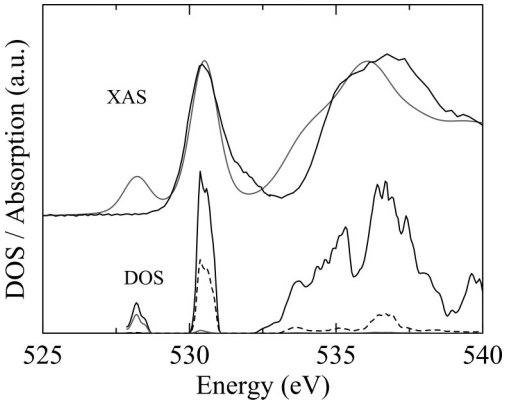

FIG. 8. Top: Comparison between measured (black) and simulated (gray) XAS spectra of Sr_2CuWO_6. Bottom: Calculated total DOS (black) and partial DOS for Cu d orbitals (gray) and W d orbitals (dashed) for Sr_2CuWO_6.

experimental XAS is missing in the calculated spectrum. From this we can conclude that the experimental absorption peak at 531.2 eV is due to the empty Cu 3d–O 2p band, pushed up in energy by the on-site Coulomb correlations, as our previous work predicted [6].

With increasing Mo content in the series, a new peak appears at around 529.4 eV, as shown as an example in Fig. 7(b) for the $x = 0.3$ sample. This peak corresponds to the empty Mo 4d–O 2p band, lower in energy compared to the W 5d–O 2p band due to weaker hybridization [6]. The ratio of the areas of the peaks related with W and Mo rises linearly with increasing Mo content. The positions in energy of the three peaks do not change with increasing Mo content in the range $x = 0$–0.5, showing that the Mo-for-W substitution does not affect the Cu 3d–O 2p band position, at least in this range of x.

The value of U for the Cu 3d electrons in these compounds could be estimated by matching the position of the calculated Cu 3d–O 2p band to the corresponding peak seen in the experimental XAS data. Figure 9 shows the DOS calculated for Sr_2CuWO_6 with different values of U. With increasing U the empty Cu 3d–O 2p band is progressively pushed up in energy: with $U = 6$ eV the Cu 3d–O 2p band is still below the W 5d–O 2p band edge, but with $U = 7$ eV, the bands practically overlap. However, with $U = 7.5$ eV the Cu 3d–O 2p band begins to emerge from the high-energy side of the W 5d–O 2p band, and with $U = 8$ eV the bands are already almost separated. Comparing these results to the experimental XAS data, we see that U of at least 7.5 eV is needed in order to push the Cu 3d–O 2p band high enough in energy above the W 5d–O 2p band.

While this comparison does not provide a very accurate value for U, it provides an estimate sufficient for the calculation of J_{ij}. According to previous computational studies using the mapping method, in general an increase in the value of U causes a decrease in the calculated values of J_{ij} [15,25,26]. However, the most interesting features, such as ratios of different exchange constants and their signs, are expected to remain relatively unchanged, as long as the value of U is reasonable. Thus in this study we settle with $U = 7.5$ eV (corresponding to $U_{\text{eff}} = U - I = 6.6$ eV), as it is the

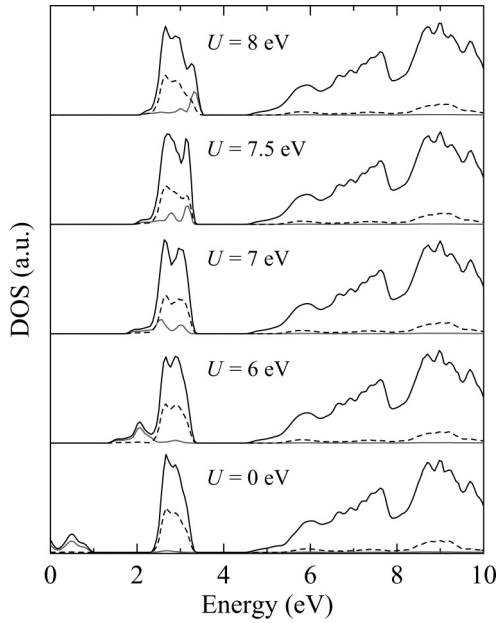

FIG. 9. Calculated total DOS (black) and partial DOS for Cu d orbitals (gray) and W d orbitals (dashed) for Sr_2CuWO_6 with U values of 0, 6, 7, 7.5, and 8 eV.

smallest value of U that can reproduce the qualitative features of the experimental XAS data. This value is also reasonable in that similar values have been used before in DFT calculations for other copper-based oxide compounds [17,19].

The total energies of the five different magnetic orderings described in Sec. III were calculated with $U = 7.5$ eV for both Sr_2CuWO_6 and Sr_2CuMoO_6. The results of the calculations are shown in Table II. All of the AFM orderings are lower in energy compared to the FM ordering, matching the AFM nature of these compounds. The values of the exchange constants J_1-J_4 calculated from the total energies as per Eqs. (8)–(11) are collected in Table II. The exchange constants are qualitatively similar for both compounds, but the absolute values are larger for Sr_2CuMoO_6 than for Sr_2CuWO_6. All the exchange constants are negative, favoring antiparallel spin arrangement. We can see that the strongest interaction is J_2, the NNN interaction in the ab plane. The NN interaction in the ab plane, J_1, is considerably weaker, but not negligible. The two interactions are slightly frustrated, as indicated by the ratio J_2/J_1, and in Sr_2CuMoO_6 ($J_2/J_1 = 2.99$) they are more frustrated than in Sr_2CuWO_6 ($J_2/J_1 = 6.23$). The NN interplanar interaction J_3 is very weak, practically zero, but the interplanar NNN interaction J_4 along the c direction is surprisingly strong, over 50% of J_2.

TABLE II. Calculated total energies of the five magnetic orderings shown in Fig. 2 (per two formula units, compared to FM), calculated exchange interactions J_1-J_4, and calculated and experimental Weiss constants θ for Sr_2CuWO_6 and Sr_2CuMoO_6.

	Sr_2CuWO_6	Sr_2CuMoO_6
FM (meV)	0.00	0.00
AFM1 (meV)	−0.12	−0.14
AFM2 (meV)	−2.45	−5.87
AFM3 (meV)	−16.19	−20.32
AFM4 (meV)	−4.27	−5.11
J_1 (meV)	−1.20	−2.90
J_2 (meV)	−7.47	−8.68
J_3 (meV)	−0.03	−0.03
J_4 (meV)	−4.21	−5.05
J_2/J_1	6.23	2.99
θ_{calc} (K)	−126	−164
θ_{exp} (K)	−116	∼−300

Finally, the order of magnitude of the calculated exchange constants can be evaluated by comparing experimental Weiss constants to those calculated using Eq. (12). These values are shown in Table II, and we can see that the calculated value for Sr_2CuWO_6 ($\theta_{calc} = -126$ K) is rather close to the experimental one ($\theta_{exp} = -116$ K), supporting our choice of U in the calculations. In case of Sr_2CuMoO_6, however, the calculated $\theta_{calc} = -164$ K is much smaller than the experimental one ($\theta_{exp} \approx -300$ K), but the trend is correct, in that the magnitude of θ increases when moving from Sr_2CuWO_6 to Sr_2CuMoO_6.

V. DISCUSSION

The experimental and computational results of this study allow us to explain the magnetic properties of the two compounds, Sr_2CuWO_6 and Sr_2CuMoO_6. First, the NPD results of Sr_2CuWO_6 showed there were no structural distortions with decreasing temperature down to 10 K. Thus, the Cu ions retain their square lattice at low temperatures, without further magnetic anisotropy in the ab plane. This permits our further analysis of the magnetic properties based on the tetragonal crystal structure. Neutron powder diffraction measurements were not performed for the high-pressure synthesized Sr_2CuMoO_6 but due to the similarity of these compounds [6], it is expected to remain tetragonal at low temperatures as well. Naturally, this would need to be verified with additional measurements.

With decreasing temperature, the magnetic susceptibilities of these two compounds begin to deviate from a Curie-Weiss type paramagnetic behavior and go through a broad maximum at T_{max}. Such a temperature maximum indicates an appearance of low-dimensional AFM correlations, because the temperature is of the order of the magnetic coupling strength [27]. Our calculations show that these correlations are caused mainly by the relatively strong and negative NNN interaction in the ab plane, J_2, slightly frustrated by the NN interaction in the ab plane, J_1. This result is in accordance with previous predictions that in such $A_2CuB''O_6$-type double perovskites J_2 is relatively strong, whereas J_1 is quite weak, but not necessarily negligible [9,10]. The temperature maximum T_{max} characterizes the energy scale of the magnetic interactions responsible for the low-dimensional behavior [28] and can thus be compared with the calculated values of J_2. We can see that the values of $|J_2| = 7.47$ meV ≈ 87 K for Sr_2CuWO_6 and $|J_2| = 8.68$ meV ≈ 101 K for Sr_2CuMoO_6 correspond rather well with the experimental values of $T_{max} = 83$ and 95 K for Sr_2CuWO_6 and Sr_2CuMoO_6, respectively.

The relatively strong and negative J_2 together with a weaker J_1 could cause a collinear AFM order to develop within the ab plane at temperatures below T_{max} (see, e.g., Ref. [6] and the references therein). However, the μSR results showed no indication of magnetic order between T_N and T_{max}, but instead appeared paramagnetic. Thus, if there is low-dimensional short-range order above T_N, it is on a very short correlation time ($\ll 10^{-10}$s), not detectable with μSR.

With further decrease in temperature, the magnetic susceptibility and μSR results confirm a long-range magnetic order taking place at T_N, notably below T_{max}. Such a suppression of T_N is commonly caused by low dimensionality and/or frustration of the spin system [27,28]. Our calculations indicate that the long-range order is due to the negative interplanar NNN interaction J_4, whereas the NN interplanar interaction J_3 is negligible. The calculated values of $|J_4| = 4.21 \approx 49$ K for Sr_2CuWO_6 and $|J_4| = 5.05 \approx 59$ K for Sr_2CuMoO_6 are somewhat higher than the values of T_N (24 and 28 K for Sr_2CuWO_6 and Sr_2CuMoO_6, respectively), but they show the correct trend, in that $|J_4|$ for Sr_2CuWO_6 is smaller than that for Sr_2CuMoO_6. Based on these results, it appears that the relatively low T_N compared to T_{max} is caused by the weakness of J_4 compared to J_2. In addition, the NNN interactions are slightly frustrated by the NN interaction J_1, which could cause additional suppression of T_N.

The T_N values determined by μSR are very similar for both of the compounds, but the measured Weiss constant is notably larger for Sr_2CuMoO_6 ($\theta \approx -300$ K) than for Sr_2CuWO_6 ($\theta = -116$ K) [6]. The "frustration index" $f = |\theta|/T_N$ is therefore $\sim$5 and $\sim$10 for Sr_2CuWO_6 and Sr_2CuMoO_6, respectively. Thus, in the case of Sr_2CuMoO_6 the magnetic interactions appear to be more frustrated than in case of Sr_2CuWO_6. In general, the absolute value of f is not necessarily an indication of magnetic frustration, as it can be affected by the low dimensionality of the magnetic interactions [27,29]. However, as both of the compounds have practically the same crystal structure [6], the increase in f from Sr_2CuWO_6 to Sr_2CuMoO_6 can be assigned to enhanced magnetic frustration. This is in accordance with our calculations, which also show that the magnetic interactions are more frustrated in Sr_2CuMoO_6 than in Sr_2CuWO_6.

The development of the local magnetic field, with critical exponents $\beta = 0.3$–0.4 as determined from the μSR results near T_N, indicates that the magnetic order below T_N in these two compounds is a regular 3D long-range order. For Ba_2CuWO_6, a similar value of $\beta = 0.35$ has been determined earlier [9]. In case of the double-perovskite lattice, the relatively strong negative NNN interactions, as found in this work, are expected to give rise to so-called "type-II" AFM order, with $k = (\frac{1}{2},0,\frac{1}{2})$ with respect to the tetragonal unit cell [30–32]. This type of AFM order has also been proposed for Ba_2CuWO_6 based on NPD measurements [9]. In our case the NPD data did not show any magnetic reflections for Sr_2CuWO_6, and thus the type of the magnetic order could not be verified. This is not surprising, as quasi-low-dimensional systems often exhibit weak magnetic reflections, even when they are magnetically ordered [33,34]. In the case of Ba_2CuWO_6, early NPD studies could not find magnetic reflections either [10]. In a later study of Ba_2CuWO_6, magnetic reflections were successfully detected at 10 K with neutron diffraction, but the ordered moment deduced from the results was only about 0.2 μ_B [9]. We estimated the detection limit for the ordered magnetic moment from our measured data, assuming the type-II AFM ordering, to be around 0.5 μ_B, implying that the ordered moment of Sr_2CuWO_6 would be less than this. The nature of the long-range magnetic order of these compounds should be verified by additional high-intensity neutron diffraction studies.

While the experimental and computational results of this study agree rather well for the most part, the Weiss constant calculated for Sr_2CuMoO_6 deviated rather notably from the experimental one, and no clear reason for this discrepancy was found. Thus, the magnetic properties of Sr_2CuMoO_6 would require additional examination, but the requirement of high-pressure synthesis conditions, and the resulting small sample size and relative impurity, makes this compound somewhat difficult to study.

VI. CONCLUSIONS

In this work we studied the low-temperature magnetic properties of Sr_2CuWO_6 and Sr_2CuMoO_6 using both experimental and computational methods. These two compounds exhibit quasi-two-dimensional magnetic properties, caused mainly by the NNN interaction within the ab plane of the tetragonal double perovskite structure. However, three-dimensional long-range magnetic order is attained at low temperatures due to a weaker but still substantial interplanar NNN interaction along the c axis. Both of the corresponding exchange constants are negative, and as the NN interactions are relatively weak, the expected magnetic long-range order is type-II AFM in the double-perovskite lattice.

While the main magnetic interaction responsible for the low-temperature long-range order is the interplanar NNN interaction, the interplanar NN interaction is negligible. This suggests that modifying the compounds in order to weaken or completely eliminate the NNN interaction along the c axis could result in a more strongly two-dimensional compound. In addition, our results show that the relative strength of the magnetic interactions and the resulting magnetic frustration in these compounds can be modified by chemical substitution. Thus, these double perovskites and other related structures could present a fruitful area of research for novel low-dimensional low-temperature magnetic properties.

ACKNOWLEDGMENTS

S.V. and M.K. acknowledge the financial support of Academy of Finland (Grant No. 255562) and H.S. and E.M. that of the MaNEP program. Neutron-diffraction-related activities (O.C.) were supported by the U.S. Department of Energy, Office of Science, Basic Energy Sciences, under Contract No. DE-AC02-06CH11357. Neutron scattering was carried out at the Spallation Neutron Source which is by the Scientific User Facilities Division, Office of Basic Energy Sciences, U.S. Department of Energy. The authors would also like to thank the POWGEN team, Ta-Lei Chou, and H. Luetkens for assistance with the NPD, XAS, and μSR measurements, respectively. The authors gratefully acknowledge computational resources provided by CSC–IT Center for Science, Espoo, Finland.

[1] R. J. Cava, J. Am. Ceram. Soc. **83**, 5 (2000).
[2] E. W. Hudson, K. M. Lang, V. Madhavan, S. H. Pan, H. Eisaki, S. Uchida, and J. C. Davis, Nature (London) **411**, 920 (2001).
[3] J. C. S. Davis and D. H. Lee, Proc. Natl. Acad. Sci. U.S.A. **110**, 17623 (2013).
[4] A. N. Yaresko, A. Y. Perlov, R. Hayn, and H. Rosner, Phys. Rev. B **65**, 115111 (2002).
[5] N. S. Kini, E. E. Kaul, and C. Geibel, J. Phys.: Condens. Matter **18**, 1303 (2006).
[6] S. Vasala, J.-G. Cheng, H. Yamauchi, J. B. Goodenough, and M. Karppinen, Chem. Mater. **24**, 2764 (2012).
[7] G. Blasse, Philips Res. Rep. **20**, 327 (1965).
[8] D. Iwanaga, Y. Inaguma, and M. Itoh, J. Solid State Chem. **147**, 291 (1999).
[9] Y. Todate, W. Higemoto, K. Nishiyama, and K. Hirota, J. Phys. Chem. Solids **68**, 2107 (2007).
[10] Y. Todate, J. Phys. Soc. Jpn. **70**, 337 (2001).
[11] A. Suter and B. M. Wojek, Phys. Procedia **30**, 69 (2012).
[12] R. Kubo, Hyperfine Interact. **8**, 731 (1981).
[13] J. Rodríguez-Carvajal, Physica B **192**, 55 (1993).
[14] D. Dai, H.-J. Koo, and M.-H. Whangbo, J. Solid State Chem. **175**, 341 (2003).
[15] H.-J. Koo and M.-H. Whangbo, Inorg. Chem. **47**, 128 (2008).
[16] Y. Fujioka, J. Frantti, and R. M. Nieminen, J. Phys. Chem. B **112**, 6742 (2008).
[17] C. Tian, A. C. Wibowo, H.-C. zur Loye, and M.-H. Whangbo, Inorg. Chem. **50**, 4142 (2011).
[18] http://elk.sourceforge.net/.
[19] V. I. Anisimov, J. Zaanen, and O. K. Andersen, Phys. Rev. B **44**, 943 (1991).
[20] C.-Y. Ren and C. Cheng, Phys. Rev. B **82**, 024404 (2010).
[21] S. J. Clark, M. D. Segall, C. J. Pickard, P. J. Hasnip, M. I. J. Probert, K. Refson, and M. C. Payne, Z. Kristallogr. **220**, 567 (2005).
[22] P. Carretta, M. Filibian, R. Nath, C. Geibel, and P. J. C. King, Phys. Rev. B **79**, 224432 (2009).
[23] R. H. Heffner, J. E. Sonier, D. E. MacLaughlin, G. J. Nieuwenhuys, G. M. Luke, Y. J. Uemura, W. Ratcliff, S.-W. Cheong, and G. Balakrishnan, Phys. Rev. B **63**, 094408 (2001).
[24] G. Materlik, J. E. Müller, and J. W. Wilkins, Phys. Rev. Lett. **50**, 267 (1983).
[25] H.-J. Koo and M.-H. Whangbo, Inorg. Chem. **47**, 4779 (2008).
[26] W.-J. Son, P. Manuel, D. Adroja, and M.-H. Whangbo, Inorg. Chem. **50**, 9400 (2011).
[27] D. C. Johnston, R. J. McQueeney, B. Lake, A. Honecker, M. E. Zhitomirsky, R. Nath, Y. Furukawa, V. P. Antropov, and Y. Singh, Phys. Rev. B **84**, 094445 (2011).
[28] R. Nath, A. A. Tsirlin, E. E. Kaul, M. Baenitz, N. Büttgen, C. Geibel, and H. Rosner, Phys. Rev. B **78**, 024418 (2008).
[29] A. P. Ramirez, Annu. Rev. Mater. Sci. **24**, 453 (1994).
[30] P. D. Battle, J. B. Goodenough, and R. Price, J. Solid State Chem. **46**, 234 (1983).
[31] E. Rodríguez, M. L. López, J. Campo, M. L. Veiga, and C. Pico, J. Mater. Chem. **12**, 2798 (2002).
[32] S. Makowski, J. A. Rodgers, P. F. Henry, J. P. Attfield, and J.-W. G. Bos, Chem. Mater. **21**, 264 (2009).
[33] K. Oka, I. Yamada, M. Azuma, S. Takeshita, K. H. Satoh, A. Koda, R. Kadono, M. Takano, and Y. Shimakawa, Inorg. Chem. **47**, 7355 (2008).
[34] P. Manuel, D. T. Adroja, P.-A. Lindgard, A. D. Hillier, P. D. Battle, W.-J. Son, and M.-H. Whangbo, Phys. Rev. B **84**, 174430 (2011).